npj | clean water

www.nature.com/npjcleanwater

ARTICLE OPEN

Check for updates

# New sustainable utilization approach of livestock manure: Conversion to dual-reaction-center Fenton-like catalyst for water purification

Yingtao Sun[1], Chun Hu[1] and Lai Lyu[1,2]✉

Rural pollution is largely caused by the accumulation of waste biomass, such as livestock manure and crop straw, which is extremely difficult to dispose of due to the simultaneous need to non-destructively treat metal and organic matter. Untreated fecal waste fluxes have contributed to more than 870,000 sanitation-related deaths annually worldwide. The existing disposal methods are accompanied by large amounts of energy and resource consumption and GHG emissions, which are not conducive to achieving the UN Sustainable Development Goals (SDGs). Herein, we pioneer a new approach to sustainable resource utilization by subjecting unprocessed livestock manure to a Dual-Reaction-Center (DRC) Fenton-like catalyst directly through the ordered bonding of intrinsic metal-organic species *via* an in situ 2-stage calcination-annealing process with zero emissions and zero pollution. The directional electron transfers along with the generated metal cation–π interactions during the resourcelized process led to the formation of electron-rich/-poor microregions. Through triggering by a small amount of hydrogen peroxide ($H_2O_2$), the removal of refractory pollutants reaches 100% within a very short time in this system, which also shows a long-term purification effect on actual wastewater, accompanied by the utilization of intrinsic energy from the pollutants and dissolved oxygen. This study is expected to advance the resource utilization of rural waste and the sustainable development of environmental factors.

*npj Clean Water* (2022)5:53 ; https://doi.org/10.1038/s41545-022-00200-2

## INTRODUCTION

Rural pollution is closely related to food security, soil and water security, global and local climate change, human diseases and the social order[1,2], and it has a profound impact on global sustainable development and is an important problem worthy of widespread attention. Fecal waste in particular has increased dramatically and has not been properly disposed of in the rural areas of some countries for a long time, causing serious environmental pollution and health risks[3]. Untreated fecal waste fluxes contributed to more than 870,000 sanitation-related deaths in 2016[4]. In China, more than $3.2 \times 10^9$ tons/year of livestock-poultry manure are produced by the breeding industry[5]. The disposal of these wastes has also increased pressure on rural development. The existing treatment methods for fecal waste, including bio gasification, composting and fermentation, often require complicated treatment processes, harsh conditions and long biological metabolism times[6,7]. The most obvious disadvantage is that these treatment processes can lead to the release of heavy metals and disease-causing microbes, the spread of odors, and large amounts of GHG emissions[4], which cause secondary damage to the environment. It is urgent for global sustainable development that we explore new, environmentally friendly disposal and resource utilization technologies for fecal waste.

In fact, fecal waste, especially livestock-poultry manure, contains a large number of useful organic and metallic substances. Chicken manure (CM), for example, contains various elements, such as Ca, Cu, Fe, Si, C, and O[8], which could provide raw components for the development and synthesis of industrial materials, including metal-organic frameworks (MOFs)[9,10] and metal-organic complex polymers (MOCPs)[11,12]. Based on their typical metal-organic coordination structures, MOFs and MOCPs are currently widely used in the chemical, environmental and energy fields. However, the industrial synthesis of these materials must rely on the addition of expensive metal species and carbon sources, accompanied by energy-intensive coprecipitation and hydrothermal processes[13–15], resulting in high consumption of resources and energy and huge environmental pressure, which is not conducive to achieving the global Millennium Development Goals (MDGs)[16,17]. Waste recycling is becoming a sustainable strategy for providing raw components for the synthesis of these materials.

In our previous work, we found that the formation of metal cation-π structures by constructing metal-organic structures on the catalyst surface was beneficial to the surface electron rearrangement, to form dual-reaction-centers (DRCs) with electron-rich/poor microregions, which drove the efficient and rapid degradation of refractory organic pollutants in the Fenton-like reaction and revolutionized the principle of the Fenton reaction by using the energy of pollutants to reduce the $H_2O_2$[18–25]. This work shows that there is a promising way to solve the problem of resource and energy consumption by applying catalysts through structural regulation. However, like other MOFs and MOCPs materials, the resource and energy-intensive synthesis stage of the catalyst is still insurmountable, which strongly violates the concept of sustainable development. Using fecal waste as a raw material to convert into an excellent Fenton-like catalyst is viewed as an innovative strategy that can simultaneously solve the fecal disposal problem and reduce the energy consumption needed for water treatment[26], even though it is a global challenge.

In this study, we have successfully implemented this sustainable strategy through the direct graphitization and functionalization of unprocessed CM to obtain high efficiency Fenton-like catalyst Cu-CM nanoparticles (CCM-Nps) through the ordered bonding of

[1]Key Laboratory for Water Quality and Conservation of the Pearl River Delta, Ministry of Education, Institute of Environmental Research at Greater Bay, Guangzhou University, Guangzhou 510006, China. [2]Institute of Rural Revitalization, Guangzhou University, Guangzhou 510006, China. ✉email: lyulai@gzhu.edu.cn

intrinsic metal-organic species with zero emissions and zero pollution for the first time, as accompanied by the fully resourcelized utilization and harmless conversion of the metallic and nonmetallic components in CM. The surface electron-rich/-poor microregions generated during the resourcelization of CM were found to be the key for using the intrinsic energy of pollutants and dissolved oxygen to achieve water purification. As a result, CCM-Nps show excellent performance in $H_2O_2$ activation and removal for a variety of organic pollutants as well as during actual wastewater treatment. The innovative transformation of CM into a high-efficiency Fenton-like catalyst has simultaneously achieved the harmless disposal of CM and efficient wastewater treatment, which has great sustainability implications.

## RESULTS

### Resourcelized conversion of chicken manure into CCM-Nps

An innovative resourcelized conversion approach to livestock manure based on an in situ 2-stage calcination-annealing process is reported here. First, the CM (the morphology and elemental content of CM are shown in Supplementary Fig. 1) was converted into a relatively purified catalyst precursor (CM-precursor) to remove most of the water and volatile substances. The CM-precursor was then calcined to remove chemically bound water, $CO_2$ and other volatile impurities. Next, the CM-precursor was impregnated with a trace copper nitrate solution and calcined again to recrystallize the CM with Cu species. The resourcelized conversion of CM to DRC catalysts was achieved through the above process. The detailed resourcelized conversion process is shown in the "Methods" section.

### Structural characteristics of CCM-Nps

The structural characteristics of the catalyst from the resourcelized conversion of CM were revealed by a series of characterization technologies. The TEM image (Fig. 1a) demonstrates that CCM-Nps possesses a typical nanosheet structure with a long strip hexagon. Two different sizes of lattice stripes were clearly observed in the HRTEM image (Fig. 1b), which corresponded to a graphene-like structure (0.65 nm) and the oxygen species of copper (0.272 nm), respectively[27–29]. The TEM elemental mapping (Fig. 1c) of CCM-Nps shows that the main elements of the nanosheet are C and O, and Cu is flocculently and amorphously distributed on its surface, which confirms the formation of carbon-based nanosheets decorated by Cu and O species. SEM images (Supplementary Fig. 2) show the nanoparticle profiles of CCM-Nps at different scales with flocculent copper species covering the surface of the C-nanosheets. These results suggest that the successful resource utilization of irregularly structured CM forms catalysts with specific structures, providing the possibility of efficient and stable pollutant degradation.

Figure 1d shows the XRD patterns of the prepared samples. The main components of the catalyst were $CaSO_4$ and $SiO_2$, which are related to the diet of the chickens. Under Cu doping, the original lattice structure did not change dramatically, except for the obvious (002) and (111) diffraction peaks of CuO appearing at $2\theta = 35.42°$ and 38.76°[30]. The results in the XRD spectra correspond to the peak position of CuO (PDF#89-5899), with an average lattice stripes size of 0.251 nm, which is slightly smaller than the lattice stripes observed by TEM. Notably, the catalyst is a composite system, so there would be deviations in the lattice size compared to the pure substance. The Raman spectra of CCM-Nps (Fig. 1e) show two evident peaks at 1355.59 $cm^{-1}$ (D band) and 1608.58 $cm^{-1}$ (G band), corresponding to carbon atoms with $sp^3$ hybridization owing to defects in or the distortion of the crystal lattice and the active $E_{2g}$ vibration of $sp^2$ hybridized carbon atoms[31], respectively, which are the typical characteristic peaks of graphene, confirming the formation of graphene-like structures on CCM-Nps. Compared with CM-Nps, the Raman spectrum of CCM-Nps is significantly enhanced in intensity and changes in position, suggesting that the introduction of Cu species is more favorable to the formation of graphene-like structures. In addition, compared with the Cu–O band (285.3 $cm^{-1}$) of the CuO (pure) sample, the characteristic peak of CCM-Nps shifted to a higher frequency (290.7 $cm^{-1}$), which suggested the conversion of the Cu–O band to the Cu–O–C band bridges due to the graphene-like nanosheet structure in the CM. This conclusion was confirmed in the FTIR spectra (Fig. 1f). The broad absorption bands centered at 1635.34 $cm^{-1}$ of CM-Nps were ascribed to the stretching vibration of C=O [v(C=O)], and the C=O group exhibits a slight shift to a higher wavenumber (1637.3 $cm^{-1}$) for CCM-Nps, which is attributed to the partial conversion of C=O to C–O and binding to Cu species to form C–O–Cu bond bridges. Moreover, one new absorption band emerged at 538 $cm^{-1}$, which is ascribed to the Cu–O– stretching and bending vibrations, confirming the formation of C–O–Cu bonding bridges[22]. The broad absorption bands centered at 3430.7 $cm^{-1}$ of CM, 3446.2 $cm^{-1}$ and 3361.3 $cm^{-1}$ of CCM-Nps were ascribed to the stretching vibration of OH [v(OH)] in the water molecules on the catalyst surface. Compared with CM-Nps, the v(–OH) bands of CCM-Nps were split from one (3430.7 $cm^{-1}$) into two (3446.2 $cm^{-1}$, 3363.2 $cm^{-1}$), and the positions of the peaks were significantly shifted, indicating that more –OH groups could be adsorbed onto the catalyst surface due to the strong interaction with the CM-precursor after Cu doping. In addition, the –OH group on CCM-Nps exhibited a significant transfer to a lower wavenumber after the adsorption of BPA, which has been shown to be due to the deprotonation of the phenolic OH group of BPA complexing with the surface Cu *via* σ bonding to the lone pairs of the oxygen atom[20].

Figure 1g shows the signals of the unpaired electrons in the prepared sample detected by EPR technology. An obvious EPR signal with a g value of 2.14 was detected for CM-Nps, indicating the presence of a large number of unpaired electrons, which suggests the possibility for CM resource utilization. For CCM-Nps, the unpaired electron signal weakened, which was attributed to the utilization of the CM electrons by the introduced Cu species through the transfer of electrons from the C-substrate to the Cu surroundings, forming an electron-rich Cu center. This observation was verified by the XPS spectra, in which a significant $Cu^+$ signal with a binding energy of 933.2 eV was observed (Fig. 1h), even if only $Cu^{2+}$ was added during the resource synthesis process. The characterization results above show that the successful resource utilization of CM has formed DRC catalysts with electron-rich/poor centers on the surface[32,33], which might be the key for displaying excellent activity in Fenton-like reactions[21].

### Innovative utilization of CCM-Nps: Wastewater purification

To investigate the performance of this structure during Fenton-like water treatment, a series of activity evaluations were performed. The DRC catalyst CCM-Nps obtained from the resource process is used for the purification of wastewater containing various emerging pollutants (Supplementary Fig. 3), including the endocrine disruptor bisphenol A (BPA), the pesticide precursor 2-chlorophenol (2-CP), the pharmaceuticals diphenhydramine (DP) and ciprofloxacin (CIP), with trace $H_2O_2$ under natural conditions. As shown in Fig. 2a, a very high degradation efficiency was obtained for all the emerging pollutants. Complete degradation was achieved within only 1 h. In particular, the refractory pharmaceutical pollutant DP could be quickly eliminated in 1 min with a degradation rate of over 90% (inset of Fig. 2a). BPA is a refractory plastic precursor that poses a huge risk to human health and needs hundreds of years to degrade in nature[34,35], and it was also quickly degraded in this novel system. In addition, efficient degradation could be achieved with various concentrations of catalyst (Supplementary Fig. 4). The excellent activity of

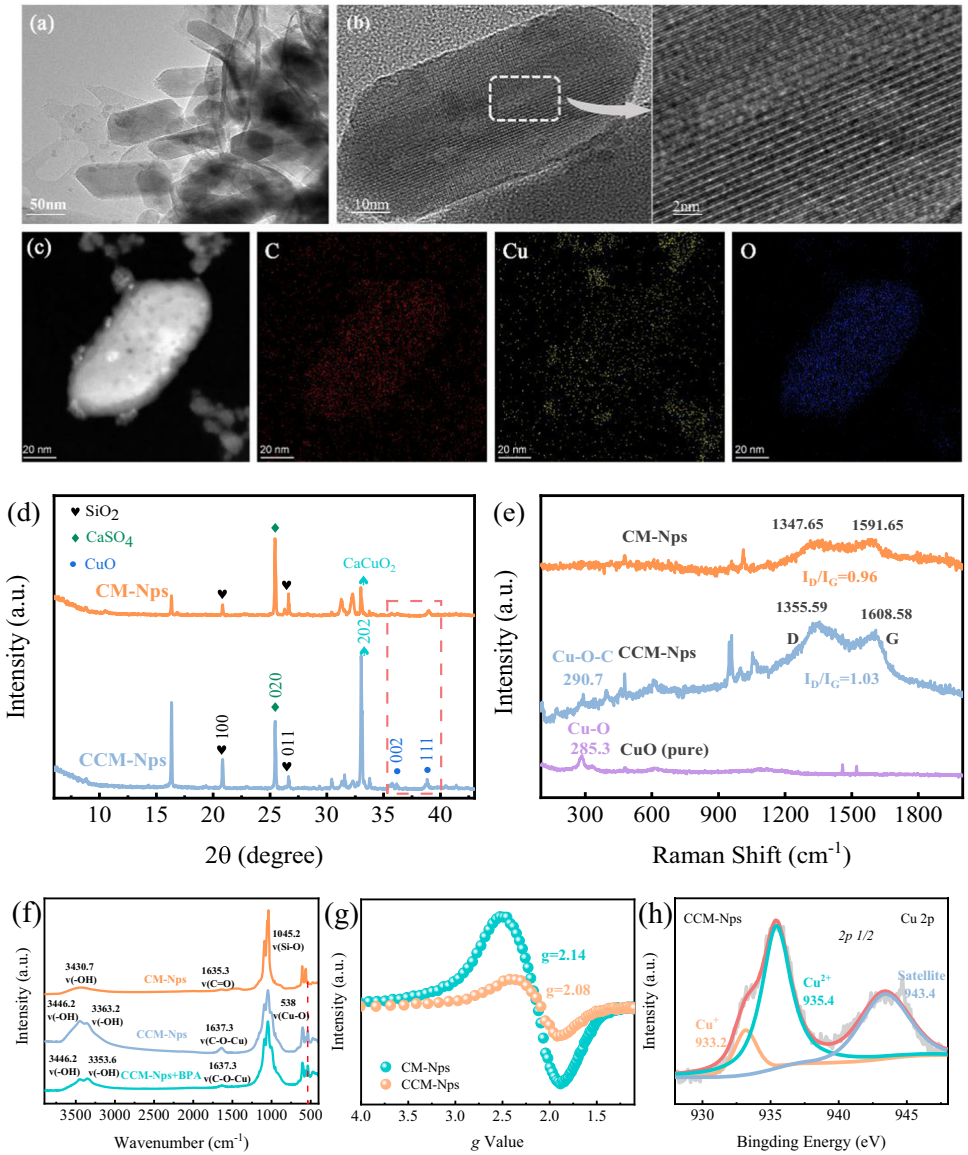


**Fig. 1 Characterization of catalysts. a** TEM image and **b** HRTEM image of CCM-Nps. **c** TEM elemental mapping of CCM-Nps. **d** XRD patterns of the prepared samples. **e** Raman spectra of CM-Nps, CCM-Nps, and CuO (pure). **f** FTIR spectra of CM-Nps, CCM-Nps and CCM-Nps after adsorption of BPA. **g** EPR spectra of CM-Nps and CCM-Nps. **h** Cu 2p XPS orbit spectrum of CCM-Nps.

CCM-Nps for pollutant degradation demonstrates the amazing potential of CM for wastewater treatment. As a comparison, the removal rate of BPA by the CM-Nps/$H_2O_2$ system was only approximately 20% within 60 min (Fig. 2b). The reaction rate of the CCM-Nps/$H_2O_2$ system is approximately 43 times higher than that of the CM/$H_2O_2$ system (inset of Fig. 2b). This system showed high pollutant removal efficiency at low concentrations of $H_2O_2$ (Fig. 2c), more than 80% of the pollutants could be removed within 60 minutes even if the concentration of $H_2O_2$ was only 2 mM. In addition, an anomaly was found in the activity evaluation: the CCM-Nps/$H_2O_2$ system had a high degradation efficiency for pollutants, and the system had a utilization of $H_2O_2$ that was several times higher than that of the conventional Fenton/Fenton-like system[36]. As shown in Fig. 2d, the consumption of $H_2O_2$ during the reaction for BPA degradation was surprisingly only 20%, and even in the comparison experiment without BPA, the consumption of $H_2O_2$ was less than 40%. These results indicate that the CM was successfully synthesized as an efficient and low-consumption Fenton-like catalyst and showed the resource utilization of the waste.

Further studies were conducted to investigate the practicality of the CCM-Nps/$H_2O_2$ system, which was applied to actual kitchen wastewater treatment (sampling points are shown in Fig. 3a, wastewater samples were obtained from malls and restaurants north of the Pearl River and west of a residential area. Additional information is shown in the Supplementary Table. 2). A comparison of the visualization of raw kitchen wastewater samples and after treatment with the CCM-Nps/$H_2O_2$ system is shown in Fig. 3b, which demonstrates excellent visual degradation of actual kitchen wastewater. Then, three-dimensional excitation emission matrix (3D-EEM) was used to detect fluorescent substances in the wastewater to evaluate the effectiveness of the CCM-Nps/$H_2O_2$ system for the treatment of this wastewater, as illustrated in Fig. 3c, d, which exhibited a high degradation efficiency. There were two principal EEM peaks in the raw kitchen wastewater (Fig. 3c). These fluorescence peaks at Ex/Em= 220–270/330–380 nm were associated with aromatic proteins (such as tyrosine and tryptophan)[37,38], which are the main components of kitchen wastewater. Both main EEM peaks disappeared after 30 min of treatment by the CCM-Nps/$H_2O_2$

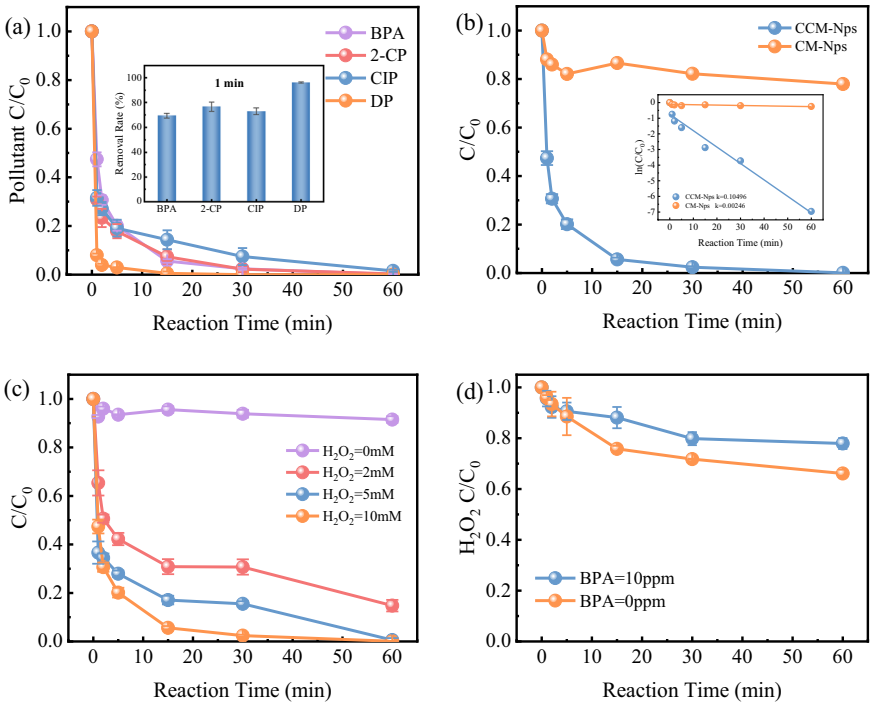


**Fig. 2 Activity evaluation under different conditions. a** Decomposition curves of different pollutants in CCM-Nps suspensions with $H_2O_2$. The inset shows the degradation rate of various pollutants within 1 min. **b** BPA degradation curves in CM-Nps and CCM-Nps suspensions with $H_2O_2$ (the inset shows the pseudo-first-order kinetic rate plots of CCM-Nps and CM-Nps Fenton-like systems). **c** Decomposition curves of BPA in CCM-Nps suspensions with different concentrations of $H_2O_2$. **d** $H_2O_2$ concentration change curve with/without BPA. Reaction conditions: [natural pH] ~ 7, [initial pollutant] = 10 mg $L^{-1}$, [initial $H_2O_2$] = 10 mM (except for c), [CCM-Nps] = 0.2 g $L^{-1}$. Two-time parallel experiments were conducted to calculate error bars in each figure.

system (Fig. 3d), indicating the efficient treatment rate of this system for kitchen wastewater and the practicality of the system.

To evaluate the stability of the CCM-Nps catalyst, a reactor was constructed to sustain the reaction and detect the degradation efficiency of BPA (Supplementary Fig. 5). As shown in Fig. 3e, after more than 900 h of continuous reaction, the experimental group still maintained the degradation rate of BPA at approximately 60%, which showed amazing stability. In contrast, the degradation rate of BPA in the control group was less than 10%. This result demonstrates the excellent stability of the CCM-Nps/$H_2O_2$ system for wastewater treatment.

Figure 3f shows the high pollutant degradation efficiency for different initial pH values in the CCM-Nps/$H_2O_2$ system. Over a wide pH range of 3.86–9.63, CCM-Nps showed strong activity for pollutant degradation. The BPA removal still reached more than 90% within 30 min even at pH values of 3.86 and 9.63. This result suggests that the activity of CCM-Nps is not significantly affected by the pH.

In actual wastewater, the existence of a large amount of high-concentration salt (anions), such as $Cl^-$, $SO_4^{2-}$, $NO_3^-$ and $PO_4^{3-}$, often results in a significant negative effect on each stage of wastewater treatment. Unexpectedly, as shown in Fig. 3g, these anions did not inhibit the activity of CCM-Nps during wastewater treatment and even significantly promoted the activity in some ion-containing systems, especially in the $NO_3^-$ and $PO_4^{3-}$-containing systems. The pollutant degradation rate exceeded 90% within only 2 min in these two systems (inset of Fig. 3g). This strong adaptability of CCM-Nps to salt is of great significance for the actual treatment of wastewater.

### Sustainable utilization mechanism of pollutants over CCM-Nps

EPR technology was used to detect radical signals during the reaction. Unusually, even in the absence of $H_2O_2$, obvious $^{\cdot}OH$ signals were detected in the CCM-Nps system at normal temperature and pressure (Fig. 4a), which demonstrated that the successful construction of DRCs on the catalyst surface could trigger the oxidation of water and lead to the utilization of electrons from water. Additionally, $O_2^{\cdot-}$ and $^1O_2$ signals were also found in this system (Fig. 4b, c), indicating that the electrons obtained from water were eventually transferred to dissolved oxygen through interfacial processes, triggering the activation of dissolved oxygen. After the addition of pollutants (BPA) to the system the $^{\cdot}OH$ signal was diminished (Fig. 4a), which showed that pollutants also acted as electron donors and competed with water, but this competition did not affect the yield of $O_2^{\cdot-}$ (Fig. 4b). In contrast, the signal intensity of $^1O_2$ was significantly increased after adding BPA, indicating that dissolved oxygen was activated. Without any assistance, this energy could only originate from the breakage and formation of chemical bonds due to the surface cleavage of pollutants. This is evidence of the energy supply from pollutants to oxygen through the created DRC surface under natural conditions and is also a reflection of the superior performance of DRC catalysts.

These results were further validated in the presence of $H_2O_2$. As shown in Fig. 4a, the signal intensity of $^{\cdot}OH$ in the CCM-Nps/$H_2O_2$ system is 5 times higher than that in the pure CCM-Nps system, which is attributed to the rapid reduction of $H_2O_2$ at the electron-rich center on the catalyst surface. In addition, the $^{\cdot}OH$ signal intensity was further enhanced after adding BPA, indicating that $H_2O_2$ acquired more electrons, which could only come from BPA. This finding reaffirms the fact that pollutants provide electrons to the system in the degradation reaction. Similarly, the $O_2^{\cdot-}$ signal intensity was also enhanced after adding BPA (Fig. 4b), but the consumption of $H_2O_2$ decreased (from 40 to 20%) (Fig. 2d), indicating that the generation of $O_2^{\cdot-}$ comes from oxygen rather than $H_2O_2$. The difference is that the $^1O_2$ signal intensity was decreased after adding BPA (Fig. 4c), suggesting that $^1O_2$ plays a key role in the degradation of pollutants.

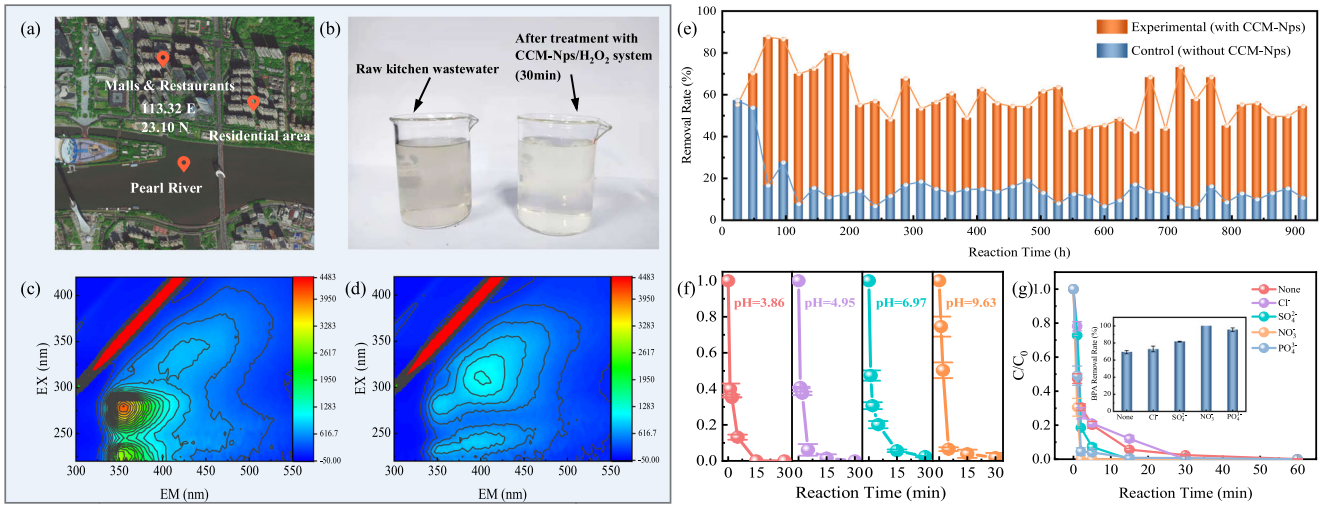


**Fig. 3 Evaluation of stability and practical applicability. a** Satellite map of actual wastewater sample sampling sites. **b** Comparison of visualization of raw kitchen wastewater samples and after 30 min reaction in CCM-Nps/$H_2O_2$ system (leave to stand and take the supernatant). Fluorescence EEMs for kitchen wastewater: **c** raw kitchen wastewater; **d** kitchen wastewater after 30 min of CCM-Nps/$H_2O_2$ system treatment. **e** Degradation stability of BPA by CCM-Nps/ $H_2O_2$ system in continuous reactor: experimental group is the effect of CCM-Nps mixed with quartz sand on the removal of BPA (quartz sand plays a fixed role to prevent the loss of catalyst), and the control group is the effect of only quartz sand on the removal of BPA. **f** Effect of initial pH values (adjusting pH by NaOH and $HNO_3$) for BPA degradation in CCM-Nps/$H_2O_2$ system. **g** Effect of different anions (1 mmol $L^{-1}$) for BPA degradation in CCM-Nps/$H_2O_2$ system, inset shows the degradation rate of CCM-Nps/ $H_2O_2$ system for BPA within 2 min under the influence of different anions. Two-time parallel experiments were conducted to calculate error bars in (**f** and **g**).

This result was verified in the radical quenching experiment (Fig. 4d). After adding TBA ($^{\bullet}OH$ quenching agent), PBQ ($O_2^{\bullet-}$ quenching agent), and FFA ($^1O_2$ quenching agent), the degradation rates of pollutants decreased by ~70, ~10, and ~90%, respectively, which suggested that $^{\bullet}OH$ and $^1O_2$ were the main active species for pollutant degradation in the CCM-Nps/$H_2O_2$ system. The addition of a quencher agent also hindered the interfacial interaction between the catalyst and pollutant, which confirmed that one important factor in achieving pollutant degradation was the fact that the pollutant actively provided electrons and energy to the catalytic system, rather than only being attacked by radicals[39].

In combination, these results suggest that during the degradation of pollutants in the CCM-Nps/$H_2O_2$ system (shown in Fig. 4e), pollutant as donors contributed energy/electrons *via* cation–$\pi$ interactions (C–O–Cu bond bridges)[40] and $\pi$–$\pi$ interactions with the electron-poor center (graphene-like nanosheets)[41] on the catalyst surface; dissolved oxygen and $H_2O_2$ act together as energy/electron acceptors in the electron-rich center (Cu species) on the catalyst surface, which generates ROS ($^{\bullet}OH$, $O_2^{\bullet-}$ and $^1O_2$, etc.) for further attack on the degradation[18–22,31,42–45]. As a consequence, the pollutants were efficiently degraded by two pathways (surface cleavage and ROS attack), achieving low consumption of $H_2O_2$ simultaneously.

Liquid Chromatograph Mass Spectrometer (LC-MS) was used to detect the decomposition products of CIP during the reaction to verify the above conclusions (the details of each decomposition product are shown in Supplementary Table 3). Additional fragments were detected as the reaction proceeded (Supplementary Fig. 6), which included the hydroxylation product and the surface cleavage product of CIP (Fig. 4f). These fragments were the result of ROS (e.g., $^{\bullet}OH$, $O_2^{\bullet-}$ and $^1O_2$) attacking CIP and the electron donation of CIP, respectively, and led to further degradation of CIP until it became $H_2O$ and $CO_2$. It is noteworthy that the hydroxylation products (m/z = 308.2, 201, and 279) mostly appeared at the beginning of the reaction, and the degradation mode of CIP changed from hydroxylation to surface cleavage over the course of the reaction, yielding special intermediates (m/z = 263, 223, 178, etc.). Therefore, $H_2O_2$ was proposed as the "first card of the domino" in the degradation reaction of the CCM-Nps/$H_2O_2$ system, in which only trace $H_2O_2$ was required to trigger the chain reaction of pollutant degradation.

## DISCUSSION

In view of these findings, a strategy to resource utilization of livestock manure into highly active and stable DRCs-catalysts is successfully implemented by ordered bonding intrinsic metal-organic species via an in situ 2-stage calcination-annealing process with zero emissions and zero pollution (Fig. 5 illustrates the implementation process of this strategy). The obtained catalyst exhibits excellent Fenton-like performance for the removal of various types of refractory pollutants (the removal rate of various refractory organics exceeds 90% within only 1 min) and shows a long-term purification effect on actual wastewater without any other external assistance. Experimental studies have uncovered the detailed mechanism of using the energy contained in pollutants for wastewater treatment. CCM-Nps is highly innovative compared to conventional heterogeneous Fenton-like catalysts.

As shown in Supplementary Table 4, it achieves the same catalytic performance as conventional catalysts while using a much lower dosage of catalyst and $H_2O_2$, which could greatly reduce resources and energy consumption in both the synthesis of catalysts and wastewater purification with catalysts. This study confirms that solid waste could be resourcelized converted into the efficient DRCs-catalyst, which has important significance for the resource utilization of rural waste and the sustainable development of environmental factors.

## METHODS

### Resourcelized conversion of chicken manure into CCM-Nps

First, the CM was converted into relatively a purified catalyst precursor (CM-precursor) after the necessary steps of natural drying and purification. The CM-precursor was then heated to a specified temperature in an atmosphere containing 10–30%

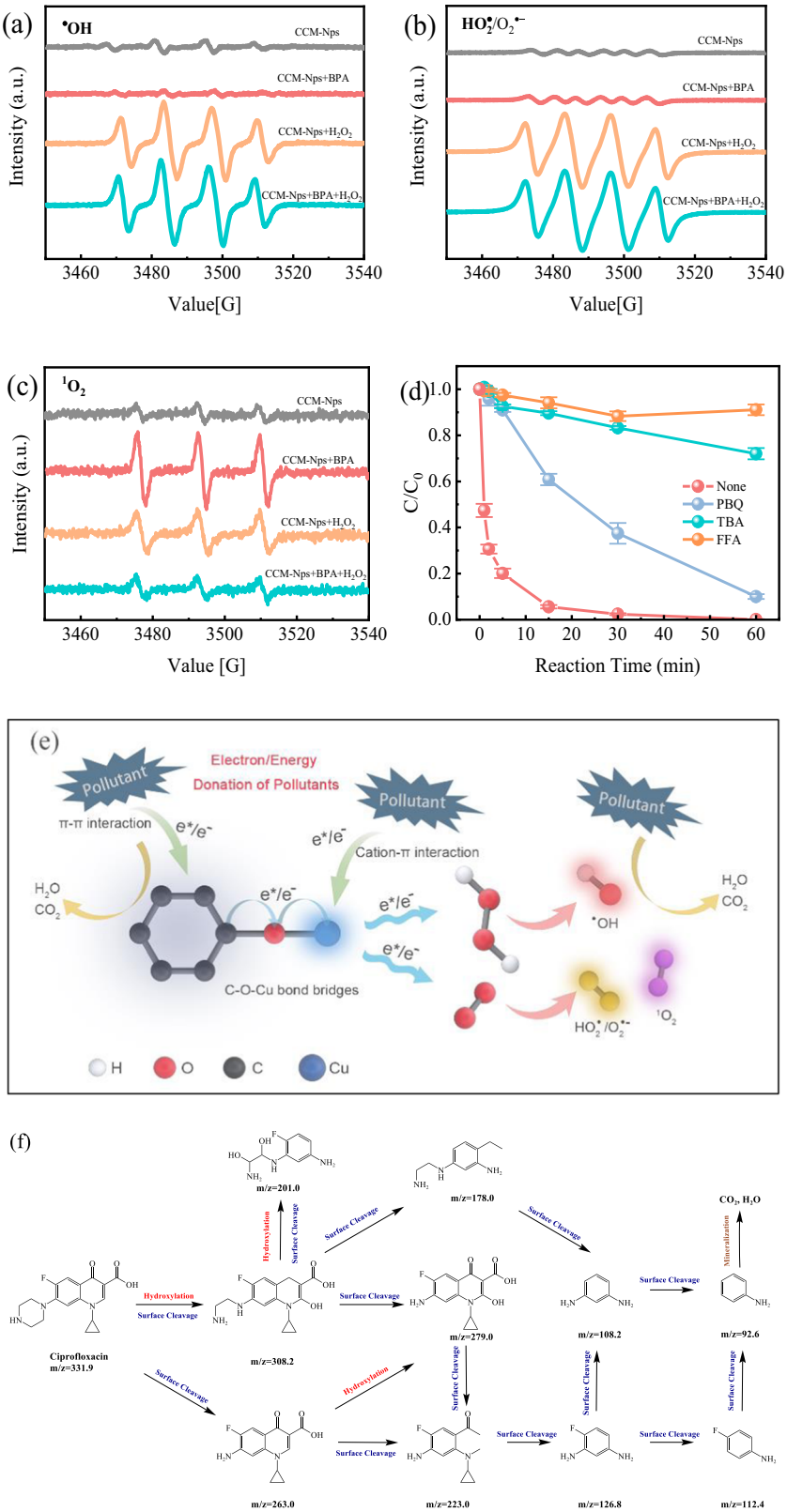


**Fig. 4 Mechanism of pollutant conversion and water purification.** BMPO/TEMP spin-trapping EPR spectra for **a** $^{\bullet}OH$, **b** $O_2^{\bullet-}$ and **c** $^1O_2$ in CCM-Nps suspensions with/without pollutants and $H_2O_2$. **d** BPA degradation curves in CCM-NPs/$H_2O_2$ system in the presence of TBA ($^{\bullet}OH$ quenching agent), PBQ ($O_2^{\bullet-}$ quenching agent), and FFA ($^1O_2$ quenching agent). Two-time parallel experiments were conducted to calculate error bars. **e** Schematic illustration of $H_2O_2$ activation and pollutant conversion on CCM-Nps surface. **f** Proposed CIP degradation pathways in the CCM-Nps/$H_2O_2$ system. Reaction conditions: natural pH ~ 7, [initial $H_2O_2$] = 10 mM, [CCM-Nps] = 0.2 g $L^{-1}$.

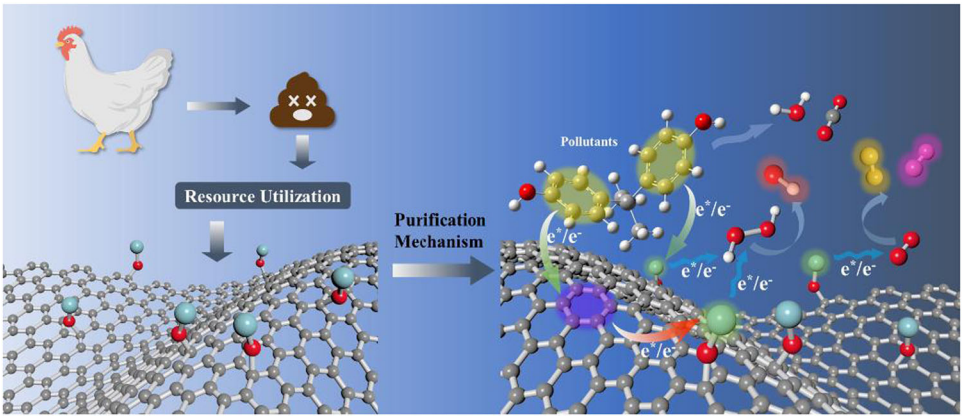


**Fig. 5 Overall pathway of resourcelized conversion and application.** Schematic illustration of resourcelized conversion of livestock manure into DRCs-catalyst.

oxygen at a set heating rate for 3–5 h, and annealed at appropriate temperature conditions. Next, hydrochloric acid solution was added to 3 g CM-precursor and stirred for 30 min. Deionized water and trace of $Cu(NO_3)_2{\cdot}3H_2O$ were added to the solution. Then the pH was adjusted to 11 through $NH_3{\cdot}H_2O$, the mixture was stirred at 80 °C in thermostat water bath to remove water, and evaporated at 140 °C in air to remove all other volatiles. Then, the obtained product was calcined at 550 °C in a muffle furnace at a heating rate of 5 °C $min^{-1}$ for 3–5 h. The resulting solid was washed with deionized water and ethanol several times to remove the soluble substances on the surface of the catalysts and dried at 100 °C for 4 h. Through these steps, CM was successfully transformed into a novel Fenton-like catalyst CCM-Nps. As control, CM-Nps was synthesized without adding $Cu(NO_3)_2{\cdot}3H_2O$.

### Characterization techniques

The surface morphology and elemental composition information for the catalysts were detected by a field emission scanning electron microscope (FE-SEM) (JSM-6700F, JEOL Co., Japan) equipped with an energy dispersive X-ray (EDX) detector system. High-resolution transmission electron microscopy (HR-TEM) (JEM-2100, JEOL Co., Japan) was performed to further analyze the morphology and crystal structures of the catalysts. The X-ray powder diffraction (XRD) patterns of the catalysts were recorded on a Philips X'Pert PRO SUPER diffractometer. Surface chemical information for the samples was collected via the X-ray photoelectron spectroscopy (XPS) (VG Multilab 2000, Thermo Electron Co., America) using monochromatic Al Kα radiation (225 W, 15 mA, 15 kV) and low-energy electron flooding for charge compensation. Solid EPR spectra were obtained using a Bruker model A300-10/12 electron paramagnetic resonance spectrometer.

### Degradation of pollutants in CCM-Nps/$H_2O_2$ system

All the experiments were carried out in a glass beaker (100 mL) containing 50 mL of 10 mg $L^{-1}$ pollutant solution (nature pH) and the whole process was kept at 35 °C (summer room temperature), the optimal dosages of catalyst powder (0.2 g $L^{-1}$) and $H_2O_2$ (10 mM) were determined according to the best activity for pollutant degradation and used in all the experiments unless otherwise specified. In a typical experiment, 50 mL of the pollutant aqueous solution with a concentration of 10 mg $L^{-1}$ and 0.01 g of the catalyst powder were placed in a beaker. Throughout the experiment, 10 mM $H_2O_2$ was added to the suspension under magnetic stirring. 2 ml aliquots were collected at given time intervals and filtered through a microporous filter (pore size 0.22 μm) for analysis.

### Specific statistical methods

Fenton-like catalysts developed in recent years are recorded and tabulated. The table details the reaction conditions for wastewater purification (the dosage of catalyst and $H_2O_2$, the concentration of pollutant, etc.) and the removal rate of the pollutant within the specific time.

The materials used and the characterization and a part of the experimental methods are discussed in detail in the Supplementary Information.

## DATA AVAILABILITY

The data that support the findings of this study are available from the Institute of Environmental Research at Greater Bay, Guangzhou. Still, restrictions apply to the availability of these data, which were used under license for the current study and are not publicly available. Data are, however, available from the authors upon reasonable request and with permission from the Institute of Environmental Research at Greater Bay, Guangzhou.

Received: 20 April 2022; Accepted: 20 September 2022;
Published online: 29 September 2022

## REFERENCES

1. Ma, T. et al. Pollution exacerbates China's water scarcity and its regional inequality. *Nat. Commun.* **11**, 650 (2020).
2. Herrera, D. et al. Upstream watershed condition predicts rural children's health across 35 developing countries. *Nat. Commun.* **8**, 881 (2017).
3. Winter, J. C. et al. The impact of on-premises piped water supply on fecal contamination pathways in rural Zambia. *npj Clean Water* **4**, 47 (2021).
4. McNicol, G. et al. Climate change mitigation potential in sanitation via off-site composting of human waste. *Nat. Clim. Change* **10**, 545–549 (2020).
5. Wang, A. D. et al. Speciation and environmental risk of heavy metals in biochars produced by pyrolysis of chicken manure and water-washed swine manure. *Sci. Rep.* **11**, 11994 (2021).
6. Loyon, L. Overview of animal manure management for beef, pig, and poultry farms in france. *Front. Sustain. Food Syst.* **2**, 36 (2018).
7. Kumar, R. R., Park, B. J. & Cho, J. Y. Application and environmental risks of livestock manure. *J. Korean Soc. Appl. Biol. Chem.* **56**, 497–503 (2013).
8. Jung, J.-M., Oh, J.-I., Baek, K., Lee, J. & Kwon, E. E. Biodiesel production from waste cooking oil using biochar derived from chicken manure as a porous media and catalyst. *Energy Convers. Manag.* **165**, 628–633 (2018).
9. Xia, T. et al. Photocatalystic degradation of organic pollutants by MOFs based materials: A review. *Chin. Chem. Lett.* **32**, 2975–2984 (2022).
10. Dai, R. et al. Tuning the primary selective nanochannels of MOF thin-film nanocomposite nanofiltration membranes for efficient removal of hydrophobic endocrine disrupting compounds. *Front. Environ. Sci. Eng.* **16**, 40 (2021).
11. Li, P. et al. Fluorescence detection of phosphate in an aqueous environment by an aluminum-based metal-organic framework with amido functionalized ligands. *Front. Environ. Sci. Eng.* **16**, 159 (2022).

12. Wang, Y., Xia, J. & Gao, Y. Decoding and quantitative detection of antibiotics by a luminescent mixed-lanthanide-organic framework. *Front. Environ. Sci. Eng.* **16**, 154 (2022).
13. Shen, B. et al. Imaging the node-linker coordination in the bulk and local structures of metal-organic frameworks. *Nat. Commun.* **11**, 2692 (2020).
14. Carné-Sánchez, A. et al. Self-assembly of metal–organic polyhedra into supramolecular polymers with intrinsic microporosity. *Nat. Commun.* **9**, 2506 (2018).
15. Hosono, N., Mochizuki, S., Hayashi, Y. & Uemura, T. Unimolecularly thick monosheets of vinyl polymers fabricated in metal–organic frameworks. *Nat. Commun.* **11**, 3573 (2020).
16. Zeng, Y. et al. Environmental destruction not avoided with the Sustainable Development Goals. *Nat. Sustain.* **3**, 795–798 (2020).
17. Griggs, D. et al. Sustainable development goals for people and planet. *Nature* **495**, 305–307 (2013).
18. Han, M. et al. In situ generation and efficient activation of $H_2O_2$ for pollutant degradation over $CoMoS_2$ nanosphere-embedded rGO nanosheets and its interfacial reaction mechanism. *J. Colloid Interface Sci.* **543**, 214–224 (2019).
19. Lyu, L. et al. Efficient destruction of pollutants in water by a dual-reaction-center Fenton-like process over carbon nitride compounds-complexed Cu(II)-$CuAlO_2$. *Environ. Sci. Technol.* **52**, 4294–4304 (2018).
20. Lyu, L. et al. Enhanced Fenton catalytic efficiency of γ-Cu-$Al_2O_3$ by σ-$Cu^{2+}$-ligand complexes from aromatic pollutant degradation. *Environ. Sci. Technol.* **49**, 8639–8647 (2015).
21. Lyu, L., Zhang, L. & Hu, C. Galvanic-like cells produced by negative charge nonuniformity of lattice oxygen on d-TiCuAl–$SiO_2$ nanospheres for enhancement of Fenton-catalytic efficiency. *Environ. Sci. Nano* **3**, 1483–1492 (2016).
22. Lyu, L. et al. Efficient Fenton-like process for organic pollutant degradation on Cu-doped mesoporous polyimide nanocomposites. *Environ. Sci. Nano* **6**, 798–808 (2019).
23. Cao, W. et al. Efficient Fenton-like process induced by fortified electron-rich O microcenter on the reduction state Cu-doped CNO polymer. *ACS Appl. Mater. Interfaces* **11**, 16496–16505 (2019).
24. Li, L. et al. Framework Cu-doped boron nitride nanobelts with enhanced internal electric field for effective Fenton-like removal of organic pollutants. *J. Mater. Chem. A* **7**, 6946–6956 (2019).
25. Lu C, et al. Sustainable micro-activation of dissolved oxygen driving pollutant conversion on Mo-enhanced zinc sulfide surface in natural conditions. *Fundam. Res.* https://doi.org/10.1016/j.fmre.2021.12.004 (2021).
26. Lu, C. et al. Dual-reaction-center catalytic process continues Fenton's story. *Front. Environ. Sci. Eng.* **14**, 5 (2020).
27. Liu, W. et al. Electrochemical $CO_2$ reduction to ethylene by ultrathin CuO nanoplate arrays. *Nat. Commun.* **13**, 1877 (2022).
28. Wang, X. et al. Morphology and mechanism of highly selective Cu(II) oxide nanosheet catalysts for carbon dioxide electroreduction. *Nat. Commun.* **12**, 794 (2021).
29. Yu, J. et al. Ultra-high thermal stability of sputtering reconstructed Cu-based catalysts. *Nat. Commun.* **12**, 7209 (2021).
30. Dong X, et al. Two-dimensional porous Cu–CuO nanosheets: Integration of heterojunction and morphology engineering to achieve high-effective and stable reduction of the aromatic nitro-compounds. *Chin. Chem. Lett*. https://doi.org/10.1016/j.cclet.2022.03.018 (2022).
31. Lyu, L. et al. 4-Phenoxyphenol-functionalized reduced graphene oxide nanosheets: A metal-free Fenton-like catalyst for pollutant destruction. *Environ. Sci. Technol.* **52**, 747–756 (2018).
32. Lyu, L. et al. The interaction of surface electron distribution-polarized Fe/polyimide hybrid nanosheets with organic pollutants driving a sustainable Fenton-like process. *Adv. Mater.* **1**, 1083–1091 (2020).
33. Zhang, H. et al. Surface oxygen vacancy inducing peroxymonosulfate activation through electron donation of pollutants over cobalt–zinc ferrite for water purification. *Appl. Catal., B* **270**, 118874 (2020).
34. Ramakrishna, M. et al. Bisphenol A—An overview on its effect on health and environment. *Biointerface Res. Appl. Chem.* **12**, 105–119 (2021).
35. Zhang, Z. et al. Fluorene-9-bisphenol is anti-oestrogenic and may cause adverse pregnancy outcomes in mice. *Nat. Commun.* **8**, 14585 (2017).
36. Lyu, L. & Hu, C. Heterogeneous Fenton catalytic water treatment technology and mechanism. *Prog. Chem.* **29**, 981–999 (2017).
37. Pramanik, B. K., Roddick, F. A. & Fan, L. Effect of biological activated carbon pretreatment to control organic fouling in the microfiltration of biologically treated secondary effluent. *Water Res.* **63**, 147–157 (2014).
38. Bu, L. et al. Characterization of dissolved organic matter during landfill leachate treatment by sequencing batch reactor, aeration corrosive cell-Fenton, and granular activated carbon in series. *J. Hazard. Mater.* **179**, 1096–1105 (2010).
39. Ren, W. et al. Activation of peroxydisulfate on carbon nanotubes: Electron-transfer mechanism. *Environ. Sci. Technol.* **53**, 14595–14603 (2019).
40. Lyu, L. et al. Enhanced polarization of electron-poor/rich micro-centers over nZVCu-Cu(II)-rGO for pollutant removal with $H_2O_2$. *J. Hazard. Mater.* **383**, 121182 (2020).
41. Cao, W. et al. l-Ascorbic acid oxygen-induced micro-electronic fields over metal-free polyimide for peroxymonosulfate activation to realize efficient multi-pathway destruction of contaminants. *J. Mater. Chem. A* **8**, 810–819 (2020).
42. Cao, W. et al. pi–pi conjugation driving peroxymonosulfate activation for pollutant elimination over metal-free graphitized polyimide surface. *J. Hazard. Mater.* **412**, 125191 (2021).
43. Cao, W., Hu, C. & Lyu, L. Efficient decomposition of organic pollutants over nZVI/$FeO_x$/$FeN_y$-anchored NC layers via a novel dual-reaction-centers-based wet air oxidation process under natural conditions. *ACS EST Eng.* **1**, 1333–1341 (2021).
44. Zhang, H. et al. Cation−π structure inducing efficient peroxymonosulfate activation for pollutant degradation over atomically dispersed cobalt bonding graphene-like nanospheres. *Appl. Catal., B* **286**, 119912 (2021).
45. Zhan, S. et al. Efficient Fenton-like process for pollutant removal in electron-rich/poor reaction sites induced by surface oxygen vacancy over cobalt–zinc oxides. *Environ. Sci. Technol.* **54**, 8333–8343 (2020).

## ACKNOWLEDGEMENTS

This work was financially supported by the National Natural Science Foundation of China (52122009, 52070046, 51838005), the Introduced Innovative R&D Team Project under the "Pearl River Talent Recruitment Program" of Guangdong Province (2019ZT08L387), the Guangdong Province Universities and Colleges Pearl River Scholar Funded Scheme (Young Scholar) and Basic and Applied Basic Research Project of Guangzhou (202102020220, 202201020163).

## AUTHOR CONTRIBUTIONS

S.Y.T. conceived and designed the experiment, performed the experiments. L.L. developed the concept. S.Y.T., H.C., and. L.L. analyzed the data, wrote and revised the paper. All of the authors provided discussion of the data and ideas and gave input on the manuscript.

## COMPETING INTERESTS

The authors declare no competing interests.

## ADDITIONAL INFORMATION

**Supplementary information** The online version contains supplementary material available at https://doi.org/10.1038/s41545-022-00200-2.

**Correspondence** and requests for materials should be addressed to Lai Lyu.

**Reprints and permission information** is available at http://www.nature.com/reprints

**Publisher's note** Springer Nature remains neutral with regard to jurisdictional claims in published maps and institutional affiliations.